arXiv:1210.5571v1 [cond-mat.supr-con] 20 Oct 2012

Nodal quasiparticle dynamics in the heavy fermion superconductor $\mathrm{CeCoIn_5}$ revealed by precision microwave spectroscopy

C. J. S. Truncik,[1] W. A. Huttema,[1] P. J. Turner,[1] S. Özcan,[2] N. C. Murphy,[1]
P. R. Carrière,[1] E. Thewalt,[1] K. J. Morse,[1] A. J. Koenig,[1] J. L. Sarrao,[3] and D. M. Broun[1]

[1] *Department of Physics, Simon Fraser University, Burnaby, BC, V5A 1S6, Canada*
[2] *Cavendish Laboratory, Madingley Road, Cambridge, CB3 0HE, United Kingdom*
[3] *Los Alamos National Laboratory, Los Alamos, New Mexico 87545, USA*

$\mathrm{CeCoIn_5}$ is a heavy fermion superconductor with strong similarities to the high-T_c cuprates, including quasi-two-dimensionality, proximity to antiferromagnetism, and probable d-wave pairing arising from a non-Fermi-liquid normal state. Experiments allowing detailed comparisons of their electronic properties are of particular interest, but in most cases are difficult to realize, due to their very different transition temperatures. Here we use low temperature microwave spectroscopy to study the charge dynamics of the $\mathrm{CeCoIn_5}$ superconducting state. The similarities to cuprates, in particular to ultra-clean $\mathrm{YBa_2Cu_3O_y}$, are striking: the frequency and temperature dependence of the quasiparticle conductivity are instantly recognizable, a consequence of rapid suppression of quasiparticle scattering below T_c; and penetration depth data, when properly treated, reveal a clean, linear temperature dependence of the quasiparticle contribution to superfluid density. The measurements also expose key differences, including prominent multiband effects and a temperature-dependent renormalization of the quasiparticle mass.

In $\mathrm{CeCoIn_5}$, evidence for d-wave pairing comes predominantly from experiments that infer the presence and location of nodes in the superconducting energy gap. This includes power laws in zero-field heat capacity[1–3] and thermal conductivity[2,3], and the field-angle dependence of heat capacity[4,5], thermal conductivity[6] and quantum oscillations in the superconducting state[7]. These experiments are supported by evidence for spin-singlet pairing (decreasing Knight shift below T_c[8,9] and Pauli-limited upper critical field[10]) and by the nature of the spin-resonance peak[11]. However, the emerging picture of $d_{x^2-y^2}$ pairing symmetry in $\mathrm{CeCoIn_5}$ is complicated by observations on the isoelectronic homologue $\mathrm{CeIrIn_5}$, which suggest a hybrid order parameter with both line nodes and point nodes[12].

Measurements of London penetration depth, λ_L, should provide a particularly clean test of nodal structure, as λ_L is a thermodynamic probe that couples preferentially to itinerant electronic degrees of freedom. However, penetration depth data on $\mathrm{CeCoIn_5}$ remain surprisingly unclear. Instead of the linear temperature dependence expected for line nodes, all penetration depth measurements to date[14–16] report temperature power laws ranging from $T^{1.2}$ to $T^{1.5}$. This presents a conundrum — mechanisms such as impurity pair-breaking[17,18] and nonlocal electrodynamics[19] should cause a crossover to *quadratic* temperature dependence, and attempts to understand the behaviour in terms of impurity physics require unrealistically high levels of disorder[20]. Here we solve this puzzle using comprehensive measurements of the frequency-dependent superfluid density, showing that the anomalous temperature power laws result from a breakdown in one of the fundamental assumptions underlying the interpretation of penetration depth measurements — that the diamagnetic contribution to the superfluid response is temperature independent. Measurements of superfluid density across a wide range of microwave frequencies reveal that the diamagnetic response (the plasma frequency) of $\mathrm{CeCoIn_5}$ *weakens* on cooling. This corresponds to an *increase* in quasiparticle effective mass that is suggestive of proximity to a quantum critical point[21,22].

In addition to thermodynamic information on the nodal structure of the pairing state, electrodynamic measurements provide a wealth of information on the scattering dynamics of thermally excited quasiparticles, particularly if carried out over a wide range of frequencies. This is of particular interest in $\mathrm{CeCoIn_5}$ because normal-state transport measurements reveal strong inelastic scattering and non-Fermi-liquid behaviour[21,23]. In the cuprates, where similarly strong scattering is observed in the normal state[24], electrodynamic measurements show a rapid collapse in quasiparticle scattering on cooling through T_c[25–27], indicating that the charge carriers couple to a spectrum of fluctuations of electronic origin, in contrast to the phonons of a conventional metal. Early measurements on $\mathrm{CeCoIn_5}$ suggest that similar behaviour occurs[2,14].

Results

Surface impedance. Measurements of surface impedance, $Z_s = R_s + \mathrm{i}X_s$, have been made at a set of discrete frequencies ranging from $\omega/2\pi = 0.13$ GHz to 19.6 GHz. As we will see below, it is only by probing the electrodynamics over such a wide range that we can isolate the contribution from low-lying quasiparticle excitations, and by doing so resolve the issue of anomalous powers laws in penetration depth. The technique used to measure Z_s is resonator perturbation: the sample, a small single crystal of $\mathrm{CeCoIn_5}$, is placed inside a resonator at a maximum in the RF magnetic field, as shown in Fig. 1. Screening currents are induced to flow on the sample surface. The depth to which fields penetrate into the sample (the skin depth δ) determines the

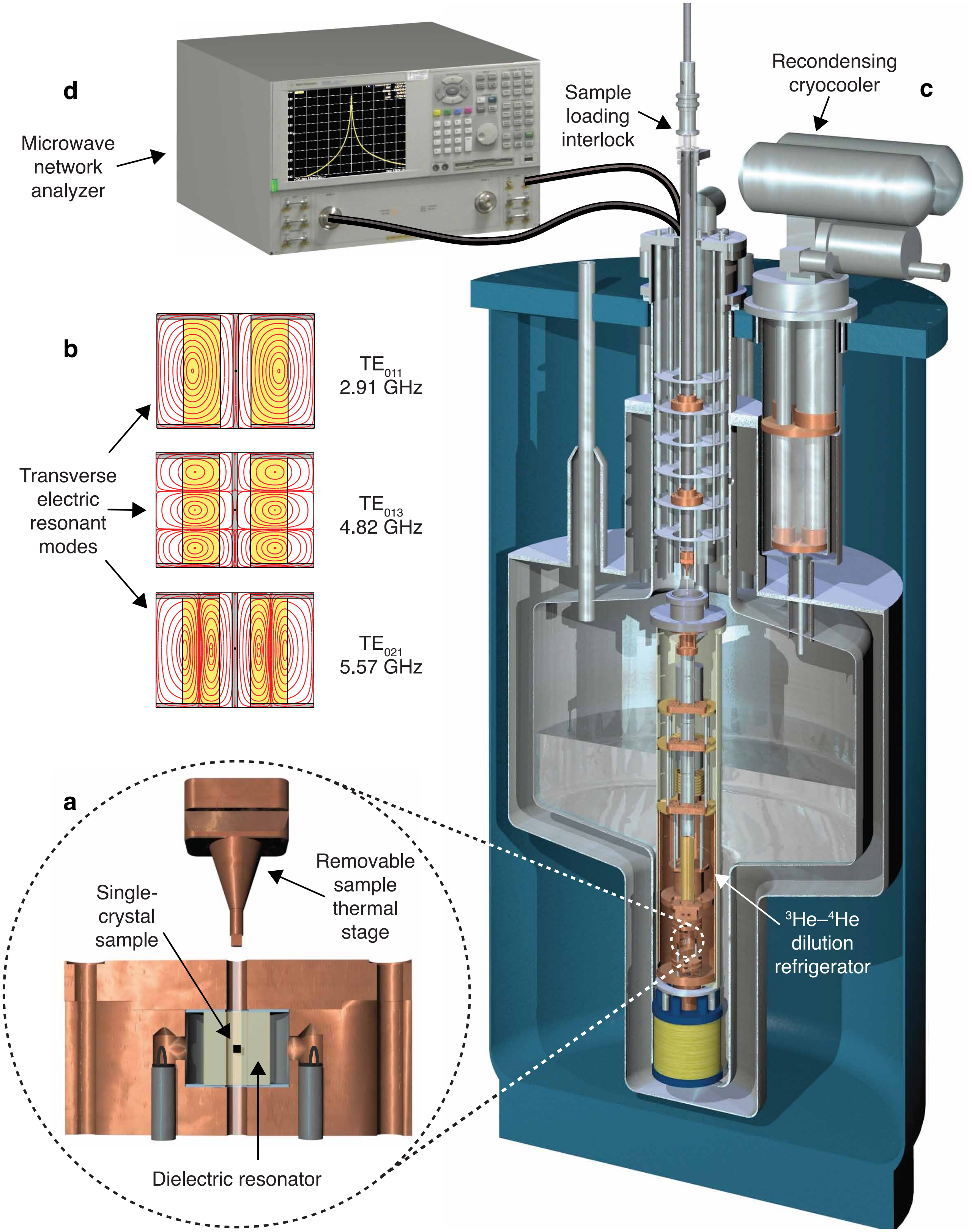

FIG. 1. **Millikelvin microwave spectroscopy.** (**a**) A platelet single crystal of CeCoIn$_5$ is mounted on a removable thermal stage and introduced into a dielectric resonator. (**b**) The resonator is excited in multiple transverse electric (TE) modes at different frequencies, all characterized by a local maximum of the RF magnetic field (red lines) at the centre of the resonator. This induces in-plane screening currents that flow across the broad faces of the CeCoIn$_5$ crystal. (**c**) The resonator is mounted below the mixing chamber of a ^{3}He–^{4}He dilution refrigerator. The sample stage is loaded from room temperature through a vacuum interlock, and can be cooled to 0.08 K. A recondensing cryocooler eliminates helium boil off. (**d**) Shifts in sample surface impedance cause changes in resonance line shape that are read out by a low-noise microwave network analyzer.

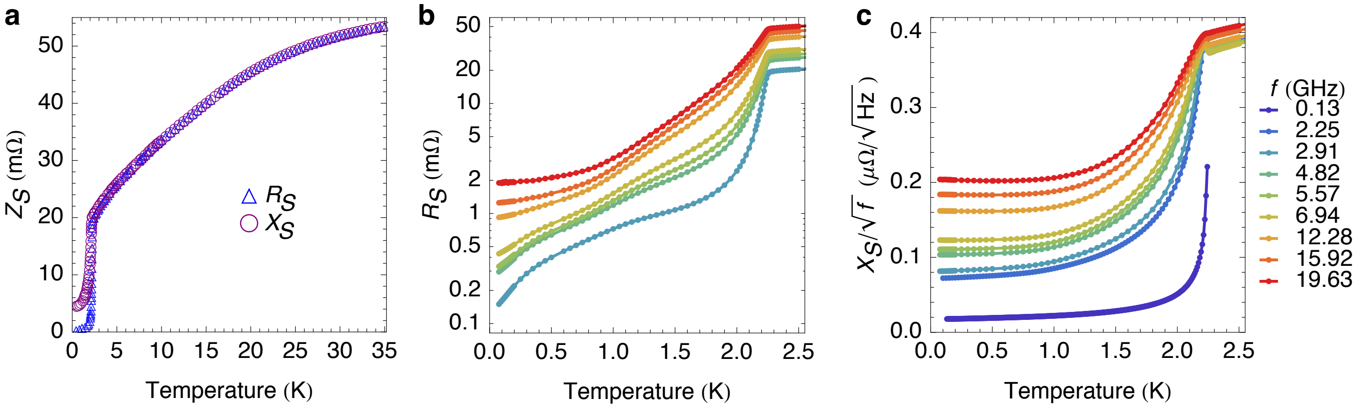

FIG. 2. **Microwave surface impedance.** (**a**) Surface impedance at 2.91 GHz, showing the results of the normal-state matching technique used to determine absolute reactance: $R_s(T)$ and $X_s(T)$ track well between $T = 10$ K and 35 K, a range in which the quasiparticle scattering rate is much greater than the measurement frequency. (**b**) Surface resistance at frequencies from 2.91 GHz to 19.6 GHz, on a logarithmic scale. Absolute surface resistance is determined by a combination of cavity perturbation and *in-situ*, resonator-based bolometry. (**c**) Surface reactance, at all frequencies measured. For clarity, $X_s(T)$ is scaled by $1/\sqrt{f}$, to factor out the expected frequency dependence well above T_c.

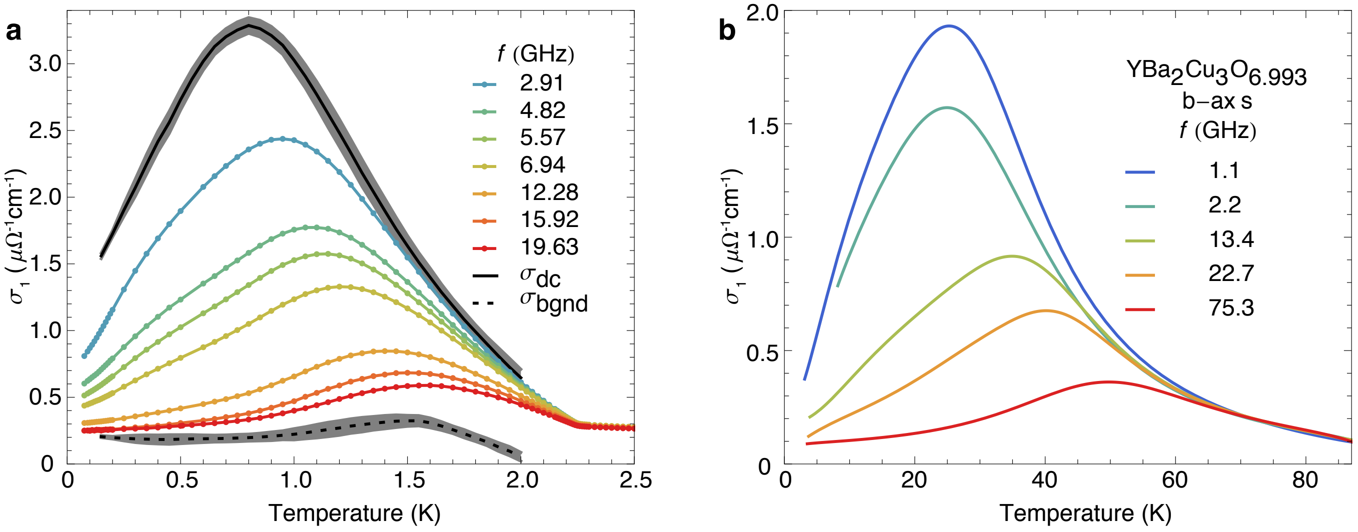

FIG. 3. **Quasiparticle conductivity of $\mathbf{CeCoIn_5}$ and $\mathbf{YBa_2Cu_3O_{6.993}}$.** (**a**) Real part of the conductivity, σ_1, of $CeCoIn_5$ as a function of temperature, for discrete frequencies from 2.91 to 19.63 GHz. Also plotted are parameters from fitting to conductivity spectra: $\sigma_{\mathrm{bgnd}}(T)$; and $\sigma_{\mathrm{dc}}(T) = \sigma_0(T) + \sigma_{\mathrm{bgnd}}(T)$. Shaded confidence bands denote standard errors in these parameters. (**b**) For comparison, the real part of the b-axis conductivity of $T_c = 89$ K $YBa_2Cu_3O_{6.993}$, as a function of temperature, at frequencies from 1.1 to 75.3 GHz (data from Ref. 13).

effective volume of the resonator and hence its resonant frequency. This provides information on the surface reactance, $X_s \approx \omega\mu_0\delta$. Although superconductors have perfect DC conductivity, the finite inertia of the electrons means that accelerating them at high frequencies requires substantial electric fields. These electric fields couple to quasiparticle excitations in the superconductor, producing a surface resistance, R_s, that grows approximately as ω^2. This dissipation is measured by monitoring the quality factor of the resonator. The complete set of surface impedance data is presented in Fig. 2.

Microwave conductivity. The complex-valued microwave conductivity, $\sigma = \sigma_1 - \mathrm{i}\sigma_2$, is obtained from the surface impedance assuming the local electrodynamic relation $\sigma = \mathrm{i}\omega\mu_0/Z_s^2$. At finite frequencies, the real part of the microwave conductivity, σ_1, is due entirely to thermally excited quasiparticles: i.e., $\sigma_1 = \mathrm{Re}\{\sigma_{\mathrm{qp}}\}$. Data for σ_1 are presented in Fig. 3a as a function of temperature. At all frequencies measured, $\sigma_1(T)$ shows an initial rise on cooling through $T_c = 2.25$ K and a broad peak at intermediate temperatures. This is the result of a sharp collapse in quasiparticle scattering below T_c that outpaces the gradual condensation of quasiparticles

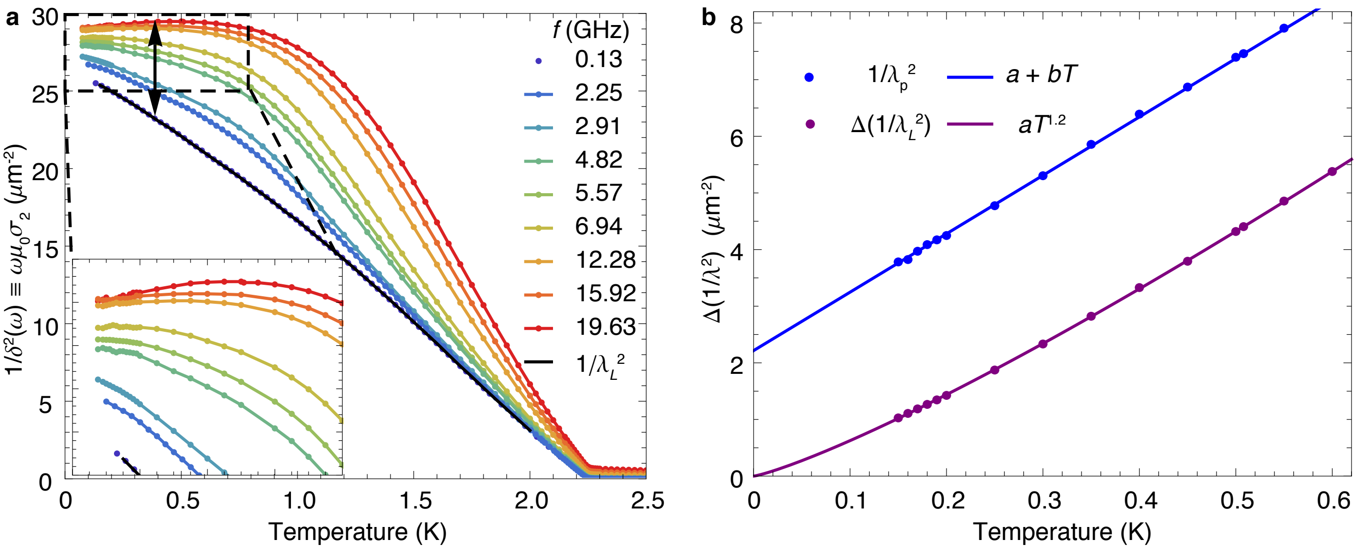

FIG. 4. **Superfluid density of CeCoIn$_5$.** (**a**) Frequency-dependent superfluid density, $1/\delta^2(\omega, T) \equiv \omega\mu_0\sigma_2(\omega, T)$, plotted as a function of temperature, for frequencies from 0.13 to 19.6 GHz. $1/\lambda_L^2(T)$, the zero-frequency limit of $1/\delta^2(\omega, T)$, is obtained from fits to complex conductivity spectra and lies on top of the 0.13 GHz data. $\lambda_L(T \to 0) = 1960$ Å. The inset shows a close-up of the low temperature region, in which the temperature slope of $1/\delta^2(\omega, T)$ *changes sign* with increasing frequency. (**b**) The temperature-dependent part of the superfluid density, $\Delta(1/\lambda_L^2) \equiv 1/\lambda_L^2(T \to 0) - 1/\lambda_L^2(T)$, follows a $T^{1.2}$ power law. The paramagnetic part of the superfluid density, $1/\lambda_p^2 \equiv 1/\delta^2(19.6\ \text{GHz}, T) - 1/\lambda_L^2(T)$, isolates the contribution from nodal quasiparticles and follows a linear temperature dependence. Its zero-temperature intercept indicates a residual, uncondensed spectral weight of 7%.

into the superfluid. For comparison, we plot the b-axis conductivity of ultra-pure YBa$_2$Cu$_3$O$_{6.993}$[13] in Fig. 3b. The qualitative similarities in $\sigma_1(\omega, T)$ between the two materials are striking, revealing a deep connection in the underlying charge dynamics that can only be present if the two materials share the same order parameter structure and spectrum of inelastic scatterers. The conductivity data provide strong support to the conjecture that these materials are different manifestations of the same correlated electron problem: two-dimensional d-wave superconductivity proximate to antiferromagnetism[1,28–30]. A quantitative analysis of the $\sigma_1(\omega, T)$ data will be carried out later in the paper, in the frequency domain.

Superfluid density. We gain additional insights into the quasiparticle dynamics from the imaginary part of the conductivity, σ_2. Although the dominant term in σ_2 comes from superconducting screening currents, thermally excited quasiparticles make a significant contribution in CeCoIn$_5$ due to their long relaxation times. Anticipating the need to separate these two components, we define a frequency-dependent superfluid density,

$$\frac{1}{\delta^2(\omega, T)} \equiv \omega\mu_0\sigma_2(\omega, T) = \frac{1}{\lambda_L^2(T)} - \omega\mu_0 \mathrm{Im}\left\{\sigma_{\mathrm{qp}}(\omega, T)\right\}. \tag{1}$$

The zero-frequency limit of $1/\delta^2(\omega)$ is the static superfluid density, $1/\lambda_L^2$. The quasiparticle contribution to $1/\delta^2(\omega)$ is strongly frequency dependent, but vanishes in the static limit. These properties allow an unambiguous separation of superfluid and quasiparticle effects, as long as data are taken over a wide range of frequency. The frequency-dependent superfluid density of CeCoIn$_5$ is plotted in Fig. 4a, for frequencies ranging from 0.13 to 19.6 GHz. We see that the frequency dependence of $1/\delta^2$ is indeed very strong and note the difficulty of isolating $1/\lambda_L^2(T)$ from a measurement at any *single* microwave frequency. $1/\lambda_L^2(T)$ has a strong temperature dependence across the whole temperature range but, as reported in previous studies, is not linear at low temperatures. This can be seen clearly in Fig. 4b, where we show that $\Delta(1/\lambda_L^2(T))$ is well described by a $T^{1.2}$ power law. Note that our experiment directly measures the *absolute* penetration depth, and therefore the curvature is not the result of uncertainties in the absolute value of $\lambda_L(T \to 0)$. To resolve this puzzle, we look more closely at what is actually measured in a penetration depth experiment. The superfluid density, $1/\lambda_L^2$, gauges the strength of the total nondecaying current density in thermal equilibrium. It consists of two parts: a diamagnetic term, $1/\lambda_d^2$, arising from *all* the conduction electrons; and a paramagnetic backflow, $1/\lambda_p^2$, caused by the thermal redistribution of quasiparticle states in the presence of a supercurrent.

$$\frac{1}{\lambda_L^2} = \frac{1}{\lambda_d^2} - \frac{1}{\lambda_p^2} \tag{2}$$

It is the second term that is sensitive to nodal structure and is where, for instance, line nodes give rise to a linear temperature dependence. In most materials $1/\lambda_d^2$ is temperature independent, making penetration depth mea-

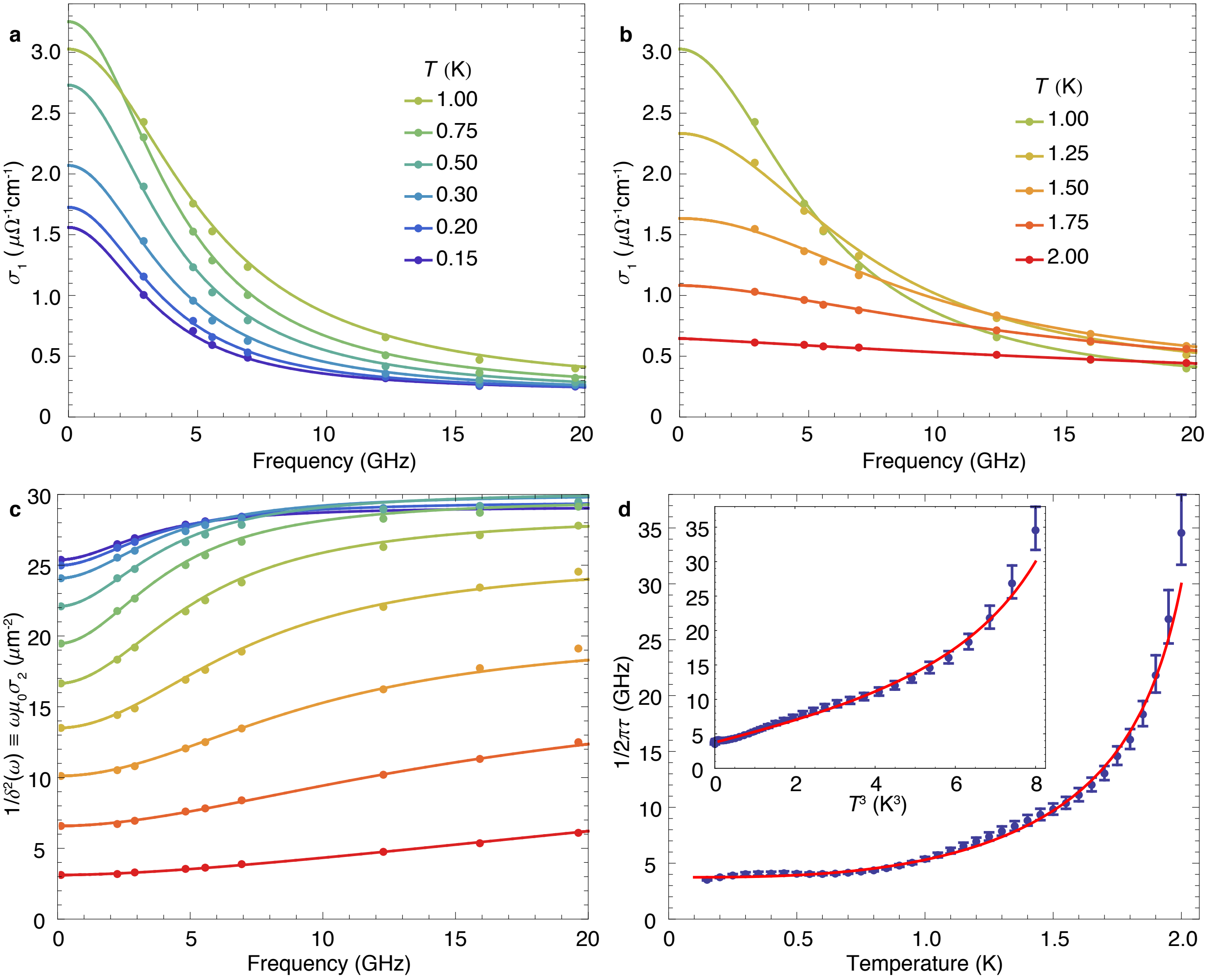

FIG. 5. **Complex conductivity spectra and model fits.** (**a**),(**b**) Real part of the conductivity as a function of frequency, at discrete temperatures. (**c**) Frequency-dependent superfluid density at the same set of temperatures as in **a** and **b**. The curves in **a, b** and **c** denote simultaneous fits to $\sigma_1(\omega)$ and $1/\delta^2(\omega)$ at each temperature, using the three-component conductivity model described in Methods. (**d**) The relaxation rate $1/\tau(T)$ obtained from the fits, as a function of temperature. The inset shows $1/\tau(T)$ as a function of T^3. Vertical bars indicate standard errors. The red lines are a fit to the function $1/\tau(T) = 1/\tau_0 + AT^3/\Delta^2(T)$, with $\Delta(T) = \Delta_0 \tanh\left(2.4\sqrt{T_c/T - 1}\right)$ used to approximate the temperature dependence of the superconducting gap energy[31].

surements a direct probe of $1/\lambda_p^2$, and therefore straightforward to interpret in terms of gap structure. However, in CeCoIn$_5$ our measurements reveal that $1/\lambda_d^2$ varies with temperature. $1/\lambda_d^2$ is proportional to the conduction electron density, n, and a Fermi surface average of the inverse of the effective mass, m^*, and can be accessed experimentally using high frequency measurements of σ_2:

$$\frac{1}{\lambda_d^2} = \mu_0 n e^2 \left\langle \frac{1}{m^*} \right\rangle_{\text{FS}} = \lim_{\omega \gg 1/\tau} \omega \mu_0 \sigma_2(\omega)\ . \qquad (3)$$

In our experiment, the condition that frequency be much larger than the quasiparticle relaxation rate, $1/\tau$, is satisfied at the lowest temperatures and highest frequencies. In Fig 4a we see that, instead of becoming temperature independent, as expected for a conventional metal, the temperature slope of $\omega\mu_0\sigma_2(\omega, T)$ *changes sign* at high frequencies, a clear indication that $1/\lambda_d^2$ has temperature dependence in CeCoIn$_5$. The observed behaviour corresponds to an effective mass that *increases* on cooling, which was raised as a possibility in earlier work[16]. This is likely a consequence of the proximity of CeCoIn$_5$ to quantum criticality[21], with related effects observed in de Haas–van Alphen studies[32]. In Fig. 4b we plot $1/\lambda_p^2(T)$, using measurements of $1/\delta^2(\omega, T)$

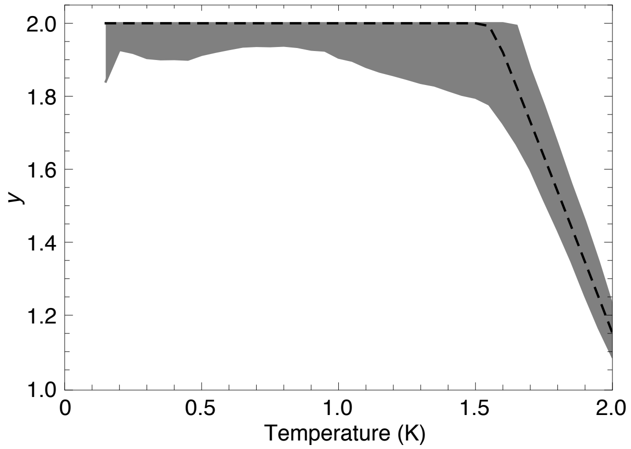

FIG. 6. **Quasiparticle conductivity frequency exponent.** The temperature dependence of the best-fit frequency exponent of the modified Drude spectrum in Eq. 4, $y(T)$. The shaded band denotes the 1σ confidence interval. $y(T)$ is constrained to lie in the range $1 < y \leq 2$.

at 19.6 GHz as a proxy for $1/\lambda_d^2$ below 0.6 K. The paramagnetic backflow term, when properly isolated, is linear in temperature, providing direct evidence that the low energy quasiparticles have a nodal spectrum and giving strong support for a d-wave pairing state.

Microwave spectroscopy. Quantitative insights into the quasiparticle dynamics are obtained from the frequency spectrum of the conductivity, plotted in Fig. 5. The collapse in scattering inferred from $\sigma_1(T)$ can now be seen directly as the narrowing of $\sigma(\omega)$ on cooling. We simultaneously fit to the real and imaginary parts of $\sigma(\omega)$ using the three-component model, Eq. 4, described in Methods. The first component is a superfluid term. Its weight is proportional to $1/\lambda_L^2(T)$, which is plotted in Fig. 4a and is tightly constrained by the 0.13 GHz data. The model also includes a quasiparticle piece, consisting of two components: a narrow, Drude-like spectrum, whose width gives the quasiparticle relaxation rate $1/\tau$; and a broad background conductivity, σ_bgnd, that accounts for a second set of rapidly relaxing excitations. The need for a multi-component spectrum is particularly apparent in the low temperature traces in Fig. 5a, which reveal narrow spectra, 3 to 4 GHz wide, riding on top of a broad background. Two of the fit parameters are plotted in Fig. 3a: $\sigma_\mathrm{dc}(T)$, the zero-frequency limit of the quasiparticle conductivity, and the broad background conductivity $\sigma_\mathrm{bgnd}(T)$. The transport relaxation rate, $1/\tau(T)$, is plotted in Fig. 5d. The conductivity frequency exponent, $y(T)$, is plotted in Fig. 6.

Discussion

Immediately above T_c, $1/2\pi\tau_n \approx 120$ GHz. (Normal-state quasiparticle lifetime, $\tau_n = \sigma_1\mu_0\lambda_0^2$, is obtained by using the zero-temperature penetration depth as a gauge of plasma frequency.) In temperature units, $\hbar/k_B\tau_n = 6$ K, several times larger than T_c, placing CeCoIn$_5$ in a similar regime of strong inelastic scattering as the cuprates[24]. On cooling into the superconducting state, $1/\tau(T)$ quickly drops into the low microwave range, where we can resolve it directly in the width of the conductivity spectra. Below 1 K, in the impurity-dominated regime, the scattering rate reaches a residual value of $1/2\pi\tau_0 = 3.5$ GHz. In the intermediate temperature range the dominant temperature dependence is well described by $1/\tau = 1/\tau_0 + T^3/\Delta^2(T)$, where in the inelastic term we allow for the gradual closing of the superconducting energy gap, $\Delta(T)$, on the approach to T_c. A cubic temperature dependence of the inelastic scattering rate is the behaviour expected when d-wave quasiparticles undergo large-momentum-transfer scattering processes, either due to the exchange of antiferromagnetic spin fluctuations[31,33], or from direct, short-range repulsion[34,35]. However, as noted by Walker and Smith[34], charge currents require Umklapp processes to relax, in order that net momentum be removed from the electron system during scattering. For d-wave quasiparticles, which at low temperatures are confined to the nodal points, momentum conservation leads to a minimum energy threshold or “Umklapp gap”. Below this threshold, Umklapp processes cannot be excited and hence at low temperatures will be frozen out. It is therefore surprising that CeCoIn$_5$ shows a predominantly T^3 dependence of the electrical relaxation rate, as this implies that the Umklapp gap, if present, is very small. Additional insights into why this may be come from the quasiparticle conductivity frequency exponent, $y(T)$. For $y = 2$, we are in the Drude limit, in which all quasiparticles relax at the same rate. Previous studies[13,36] have shown that $y < 2$ works well in capturing the phenomenology of d-wave superconductors, in which the quasiparticle relaxation rate has a strong energy dependence due to the Dirac-cone structure of the d-wave quasiparticle spectrum[18,37,38]. Below 1.5 K, the best-fit value of $y(T)$ sits at the Drude limit, $y = 2$. This is quite surprising, as it implies that all low energy quasiparticles relax at approximately the same rate — the energy-dependent scattering expected for d-wave quasiparticles appears to be absent. Above 1.5 K, $y(T)$ drops quickly, falling below 1.2 on the approach to T_c. This indicates a rapidly broadening distribution of quasiparticle relaxation rates at higher energies, possibly associated with the development of hot spots on the Fermi surface due to spin-fluctuation scattering.

The explanation for these observations (coexisting narrow and broad conductivity spectra; the insignificant Umklapp gap; and energy-independent impurity scattering) is likely related to the multiband nature of CeCoIn$_5$. Parts of the Fermi surface that are not fully gapped will provide additional phase space for recoil at low energies. This will relax the constraints that lead both to the Umklapp gap and the expectation of strongly energy-dependent scattering in a d-wave superconductor. Regarding the coexistence of broad and narrow spectral components in the quasiparticle conductivity, a broad distribution of scattering rates will naturally arise when there is a strong variation of effective mass over the Fermi surface, as occurs in CeCoIn$_5$[7,39]. Narrow conductivity spectra then correspond to heavy quasiparticles and broad spectra to light ones. The plots of $\sigma_{\rm dc}(T)$ and $\sigma_{\rm bgnd}(T)$ in Fig. 3a indicate how the partitioning between heavy and light electrons is played out, and support similar conclusions drawn from a combined analysis of heat capacity and thermal conductivity data[3]. Our experiment shows that the heavy quasiparticles experience a large decrease in scattering below T_c, and participate strongly in forming the superfluid, with only 7% spectral weight remaining uncondensed as $T \to 0$. The light quasiparticles undergo a much smaller decrease in scattering and have a large residual conductivity at low temperatures. This suggests that the spectrum of fluctuations responsible for inelastic scattering, mass enhancement, and superconducting pairing couples strongly to the heavy parts of the Fermi surface, but much less efficiently to the light band.

Our results provide a new window into the low energy charge dynamics of CeCoIn$_5$ and uncover a complex interplay between *d*-wave superconductivity, multiband physics and quantum criticality. The phenomena revealed can only be understood using measurements over a wide frequency range. Many of the features are strongly reminiscent of the cuprates, confirming a close connection between these two classes of material. An important difference is the observation of temperature-dependent quasiparticle mass, which not only resolves the issue of anomalous power laws in London penetration depth, but shows that quantum criticality is not completely circumvented by the onset of superconductivity[40].

Methods

Surface impedance. Phase-sensitive measurements of microwave surface impedance, $Z_s = R_s + {\rm i}X_s$, were made using resonator perturbation techniques, with temperature-dependent changes in Z_s obtained from resonator frequency, f_0, and resonant bandwidth, f_B, using the cavity perturbation approximation[41] $\Delta Z_s = \Gamma\left(\Delta f_B(T)/2 - {\rm i}\Delta f_0(T)\right)$. Here Γ is a resonator constant determined empirically from the known DC resistivity of CeCoIn$_5$.[42] At the lowest frequency, 0.13 GHz, surface reactance was measured using a tunnel-diode oscillator and was previously published in Ref. 16. At all other frequencies, surface impedance was measured using dielectric-resonator techniques, in a dilution-refrigerator-based variant of the apparatus described in Ref. 41. The *absolute* surface resistance was obtained at each frequency using an *in-situ* bolometric technique, by detecting the synchronous rise in temperature when the sample was subjected to a microwave field of known, time-varying intensity[43]. Thermal expansion effects make a small contribution to the apparent surface reactance, $\Delta X_s^{\rm th} \approx -\frac{\omega\mu_0 c}{2}\beta(T)$, where c is the thickness of the sample and $\beta(T)$ is the volume coefficient of thermal expansion. This was corrected for using thermal expansion data from Ref. 44.

Absolute surface reactance. The absolute surface reactance was obtained at 2.91 GHz by matching $R_s(T)$ and $X_s(T)$ between 10 K and 35 K, a temperature range in which the imaginary part of the normal-state conductivity is small and $R_s = X_s = \sqrt{\omega\mu_0\rho_{\rm dc}/2}$. To a first approximation, $X_s \approx \omega\mu_0\lambda_L$ is used to obtain the surface reactance at the other frequencies. This estimate is refined by taking into account the quasiparticle contribution to X_s. We carry this procedure out at $T = 0.1$ K, using the following self-consistent method:

1. The quasiparticle contribution to σ_2 is initially set to zero, so that $\sigma_2(\omega)$ arises purely from the superfluid conductivity, $\sigma_s = 1/{\rm i}\omega\mu_0\lambda_L^2$, with λ_L obtained from the 2.91 GHz X_s data.

2. The local electrodynamic relation, $Z_s = \sqrt{{\rm i}\omega\mu_0/\sigma}$, is used to obtain $X_s(\omega)$ from the measured $R_s(\omega)$ and the *calculated* $\sigma_2(\omega)$. This step is carried out without any explicit knowledge of $\sigma_1(\omega)$.

3. From $X_s(\omega)$ and $R_s(\omega)$ we obtain $\sigma_1(\omega)$, again using the local electrodynamic relation.

4. A Drude-like spectrum, $\sigma_1^{\rm qp}(\omega) = \sigma_0/(1+\omega^2\tau^2) + \sigma_{\rm bgnd}$, is fit to $\sigma_1(\omega)$.

5. The corresponding imaginary part, $\sigma_2^{\rm qp}(\omega) = \sigma_0\omega\tau/(1+\omega^2\tau^2)$, provides an estimate of the *quasiparticle* contribution to $\sigma_2(\omega)$.

6. The total imaginary conductivity is the sum of $\sigma_2^{\rm qp}(\omega)$, and a superfluid term of the same form as in step 1, but with λ_L adjusted to make $\sigma_2(\omega)$ consistent with the directly determined value of X_s at 2.91 GHz.

7. The refined estimate of $\sigma_2(\omega)$ is inserted into step 2, and the procedure is iterated to self consistency.

Microwave conductivity. The complex microwave conductivity, $\sigma_1(\omega) - {\rm i}\sigma_2(\omega)$, is obtained from the surface impedance using the local electrodynamic relation. At each temperature, the real and imaginary parts of σ are simultaneously fit to a three-component model consisting of a superfluid term; a broad background conductivity; and a narrow, Drude-like spectrum:

$$\sigma(\omega) = \frac{1}{{\rm i}\omega\mu_0\lambda_L^2} + \sigma_{\rm bgnd} + \left(\frac{\sigma_0}{1+(\omega\tau)^y} - {\rm i}\sigma_{\rm KK}(\omega;\sigma_0,\tau,y)\right). \quad (4)$$

The parameters of the model are: the superfluid density, $1/\lambda_L^2(T)$; the background conductivity, $\sigma_{\rm bgnd}(T)$; the magnitude of the Drude-like spectrum, $\sigma_0(T)$; the relaxation time, $\tau(T)$; and the conductivity exponent, $y(T)$, constrained to the interval $1 < y \leq 2$. $\sigma_{\rm KK}(\omega)$ denotes the imaginary part of the Drude-like spectrum, obtained using a Kramers–Krönig transform.

Samples. High quality single crystals of CeCoIn$_5$ were grown by a self-flux method in excess In[1,23]. The microwave measurements were carried out on a mm-sized platelet with naturally formed, mirror-like *a*–*b* plane faces. This sample was the same as that used in Ref. 16. The width of the (003) x-ray rocking curve was 0.014°, indicating high crystallinity. Electron-probe microanalysis gives an average composition of $\rm Ce_{1.02(1)}Co_{0.99(1)}In_{4.99(1)}$, homogeneously throughout the bulk of the crystal, indicating that the samples are single-phase and highly stoichiometric.

---

[1] Petrovic, C. *et al.* Heavy-fermion superconductivity in CeCoIn$_5$ at 2.3 K. *J. Phys. Condens. Matter* **13**, L337–L342 (2001).

[2] Movshovich, R. *et al.* Unconventional superconductivity in CeIrIn$_5$ and CeCoIn$_5$: specific heat and thermal conductivity studies. *Phys. Rev. Lett.* **86**, 5152–5155 (2001).

[3] Tanatar, M. A. *et al.* Unpaired electrons in the heavy-fermion superconductor CeCoIn$_5$. *Phys. Rev. Lett.* **95**, 067002 (2005).

[4] Aoki, H. *et al.* Field-angle dependence of the zero-energy

density of states in the unconventional heavy-fermion superconductor CeCoIn_5. *J. Phys. Condens. Matter* **16**, L13–L19 (2004).

[5] An, K. *et al.* Sign reversal of field-angle resolved heat capacity oscillations in a heavy fermion superconductor CeCoIn_5 and $d_{x^2-y^2}$ pairing symmetry. *Phys. Rev. Lett.* **104**, 037002 (2010).

[6] Izawa, K. *et al.* Angular position of nodes in the superconducting gap of quasi-2D heavy-fermion superconductor CeCoIn_5. *Phys. Rev. Lett.* **87**, 057002 (2001).

[7] Settai, R. *et al.* Quasi-two-dimensional Fermi surfaces and the de Haas–van Alphen oscillation in both the normal and superconducting mixed states of CeCoIn_5. *J. Phys. Condens. Matter* **13**, L627–L634 (2001).

[8] Curro, N. *et al.* Anomalous NMR magnetic shifts in CeCoIn_5. *Phys. Rev. B* **64**, 180514R (2001).

[9] Kohori, Y. *et al.* NMR and NQR studies of the heavy fermion superconductors CeTIn_5 (T=Co and Ir). *Phys. Rev. B* **64**, 134526 (2001).

[10] Tayama, T. *et al.* Unconventional heavy-fermion superconductor CeCoIn_5: dc magnetization study at temperatures down to 50 mK. *Phys. Rev. B* **65**, 180504 (2002).

[11] Stock, C., Broholm, C., Hudis, J., Kang, H. & Petrovic, C. Spin Resonance in the *d*-wave Superconductor CeCoIn_5. *Phys. Rev. Lett.* **100**, 087001 (2008).

[12] Shakeripour, H., Tanatar, M., Li, S., Petrovic, C. & Taillefer, L. Hybrid gap structure of the heavy-fermion superconductor CeIrIn_5. *Phys. Rev. Lett.* **99**, 187004 (2007).

[13] Harris, R. *et al.* Phenomenology of $\hat{a}$-axis and $\hat{b}$-axis charge dynamics from microwave spectroscopy of highly ordered $\mathrm{YBa_2Cu_3O_{6.50}}$ and $\mathrm{YBa_2Cu_3O_{6.993}}$. *Phys. Rev. B* **74**, 104508 (2006).

[14] Ormeno, R. J., Sibley, A., Gough, C. E., Sebastian, S. & Fisher, I. R. Microwave conductivity and penetration depth in the heavy fermion superconductor CeCoIn_5. *Phys. Rev. Lett.* **88**, 047005 (2002).

[15] Chia, E. E. M. *et al.* Nonlocality and strong coupling in the heavy fermion superconductor CeCoIn_5: A penetration depth study. *Phys. Rev. B* **67**, 014527 (2003).

[16] Özcan, S. *et al.* London penetration depth measurements of the heavy-fermion superconductor CeCoIn_5 near a magnetic quantum critical point. *Europhys. Lett.* **62**, 412–418 (2003).

[17] Prohammer, M. & Carbotte, J. P. London penetration depth of *d*-wave superconductors. *Phys. Rev. B* **43**, 5370–5374 (1991).

[18] Hirschfeld, P. J. & Goldenfeld, N. Effect of strong scattering on the low-temperature penetration depth of a *d*-wave superconductor. *Phys. Rev. B* **48**, 4219–4222 (1993).

[19] Kosztin, I. & Leggett, A. Nonlocal effects on the magnetic penetration depth in *d*-wave superconductors. *Phys. Rev. Lett.* **79**, 135–138 (1997).

[20] Kogan, V. G., Prozorov, R. & Petrovic, C. Superfluid density in gapless superconductor CeCoIn_5. *J. Phys. Condens. Matter* **21**, 102204 (2009).

[21] Sidorov, V. A. *et al.* Superconductivity and quantum criticality in CeCoIn_5. *Phys. Rev. Lett.* **89**, 157004 (2002).

[22] Paglione, J. P. *et al.* Nonvanishing energy scales at the quantum critical point of CeCoIn_5. *Phys. Rev. Lett.* **97**, – (2006).

[23] Kim, J. S., Alwood, J., Stewart, G. R., Sarrao, J. L. & Thompson, J. D. Specific heat in high magnetic fields and non-Fermi-liquid behavior in CeMIn_5 (M=Ir, Co). *Phys. Rev. B* **64**, 134524 (2001).

[24] Varma, C. M., Littlewood, P. B., Schmitt-Rink, S., Abrahams, E. & Ruckenstein, A. E. Phenomenology of the normal state of Cu-O high-temperature superconductors. *Phys. Rev. Lett.* **63**, 1996–1999 (1989).

[25] Nuss, M. C., Mankiewich, P. M., O'Malley, M. L., Westerwick, E. H. & Littlewood, P. B. Dynamic conductivity and "coherence peak" in $\mathrm{YBa_2Cu_3O_7}$ superconductors. *Phys. Rev. Lett.* **66**, 3305–3308 (1991).

[26] Bonn, D. A., Dosanjh, P., Liang, R. & Hardy, W. N. Evidence for rapid suppression of quasiparticle scattering below T_c in $\mathrm{YBa_2Cu_3O_{7-\delta}}$. *Phys. Rev. Lett.* **68**, 2390–2393 (1992).

[27] Hosseini, A. *et al.* Microwave spectroscopy of thermally excited quasiparticles in $\mathrm{YBa_2Cu_3O_{6.99}}$. *Phys. Rev. B* **60**, 1349–1359 (1999).

[28] Scalapino, D. J., Loh, E. & Hirsch, J. E. *d*-wave pairing near a spin-density-wave instability. *Phys. Rev. B* **34**, 8190–8192 (1986).

[29] Scalapino, D. J. The case for $d_{x^2-y^2}$ pairing in the cuprate superconductors. *Phys. Rep.* **250**, 330–365 (1995).

[30] Monthoux, P. & Lonzarich, G. G. *p*-wave and *d*-wave superconductivity in quasi-two-dimensional metals. *Phys. Rev. B* **59**, 14598 (1999).

[31] Duffy, D., Hirschfeld, P. J. & Scalapino, D. J. Quasiparticle lifetimes in a $d_{x^2-y^2}$ superconductor. *Phys. Rev. B* **64**, 224522 (2001).

[32] McCollam, A., Julian, S. R., Rourke, P. M. C., Aoki, D. & Flouquet, J. Anomalous de Haas–van Alphen oscillations in CeCoIn_5. *Phys. Rev. Lett.* **94**, 186401 (2005).

[33] Quinlan, S. M., Scalapino, D. J. & Bulut, N. Superconducting quasiparticle lifetimes due to spin-fluctuation scattering. *Phys. Rev. B* **49**, 1470–1473 (1994).

[34] Walker, M. B. & Smith, M. F. Quasiparticle-quasiparticle scattering in high-T_c superconductors. *Phys. Rev. B* **61**, 11285–11288 (2000).

[35] Dahm, T., Hirschfeld, P. J., Scalapino, D. J. & Zhu, L. Nodal quasiparticle lifetimes in cuprate superconductors. *Phys. Rev. B* **72** (2005).

[36] Turner, P. J. *et al.* Observation of weak-limit quasiparticle scattering via broadband microwave spectroscopy of a *d*-wave superconductor. *Phys. Rev. Lett.* **90**, 237005 (2003).

[37] Hirschfeld, P. J., Putikka, W. O. & Scalapino, D. J. *d*-wave model for microwave response of high-T_c superconductors. *Phys. Rev. B* **50**, 10250–10264 (1994).

[38] Schachinger, E. & Carbotte, J. Residual absorption at zero temperature in *d*-wave superconductors. *Phys. Rev. B* **67**, 134509 (2003).

[39] Hall, D. *et al.* Fermi surface of the heavy-fermion superconductor CeCoIn_5: The de Haas–van Alphen effect in the normal state. *Phys. Rev. B* **64**, 212508 (2001).

[40] Laughlin, R. B., Lonzarich, G. G., Monthoux, P. & Pines, D. The quantum criticality conundrum. *Adv. Phys.* **50**, 361–365 (2001).

[41] Huttema, W. A. *et al.* Apparatus for high-resolution microwave spectroscopy in strong magnetic fields. *Rev. Sci. Instrum.* **77**, 023901 (2006).

[42] Bauer, E. D. *et al.* Thermodynamic and transport investigation of $\mathrm{CeCoIn}_{5-x}\mathrm{Sn}_x$. *Phys. Rev. B* **73**, 245109 (2006).

[43] Turner, P. *et al.* Bolometric technique for high-resolution broadband microwave spectroscopy of ultra-low-loss samples. *Rev. Sci. Instrum.* **75**, 124–135 (2004).

[44] Takeuchi, T. *et al.* Thermal expansion and magnetostriction studies in a heavy-fermion superconductor, CeCoIn_5.

J. Phys. Condens. Matter **14**, L261–L266 (2002).

Acknowlegdements

Research support for the experiments was provided by the Natural Science and Engineering Research Council of Canada and the Canadian Foundation for Innovation. Research support for sample preparation was provided by the Division of Materials Science and Engineering of the U.S. Department of Energy Office of Basic Energy Sciences.

Author contributions

P.J.T., W.A.H., C.J.S.T., S.Ö., P.R.C., E.T., N.C.M., K.J.M., A.J.K. and D.M.B. designed and set up the dilution-refrigerator-based systems for microwave spectroscopy. C.J.S.T., W.A.H., P.J.T., S.Ö., N.C.M. and D.M.B. carried out the experiments. C.J.S.T. carried out the data analysis. J.L.S. prepared the sample of $\mathrm{CeCoIn_5}$. D.M.B. wrote the paper and supervised the project.

Additional information

Competing financial interests. The authors declare no competing financial interests.